Pergamon

Int. J. Heat Mass Transfer. Vol. 39, No. 17, pp. 3567–3579, 1996
Copyright © 1996 Elsevier Science Ltd
Printed in Great Britain. All rights reserved
0017–9310/96 $15.00 + 0.00

PII: S0017–9310(96)00041–5

A scaling analysis of the unidirectional solidification of a binary alloy

MATTHEW JOHN M. KRANE and FRANK P. INCROPERA

Heat Transfer Laboratory, School of Mechanical Engineering, Purdue University, West Lafayette, IN 47907, U.S.A.

(*Received* 7 *November* 1995 *and in final form* 30 *January* 1996)

Abstract—A scaling analysis of the conservation equations for momentum, heat and species transport inside the solidifying mushy zone of a binary alloy is performed to examine systematically common assumptions and predict general behavior of the mixture during freezing. Several terms in the momentum equation are found to be negligible throughout the solidifying domain, and the use of D'Arcy's law to approximate the momentum equations in the mushy zone is found to be valid except in the region near the liquidus isotherm. A criterion is developed to define this region, and the dependence of the streamfunction and buoyancy driven velocity on material properties and fraction solid is determined. The energy equation is examined to provide scaling laws for the mushy zone and solid region thicknesses, as well as the transient chill wall temperature. Advection is shown to dominate solute transport throughout the mush, although, in the denser regions of the solid–liquid region, liquid velocities are so small as to have a negligible effect on macrosegregation. Numerical calculations performed for Pb–Sn and Al–Mg alloys at different cooling rates confirm trends suggested by the scaling analysis. Copyright © 1996 Elsevier Science Ltd.

1. INTRODUCTION

Through its influence on phenomena such as solute redistribution and remelting, liquid flow during solidification of an off-eutectic alloy can significantly affect the thermal, electrical and mechanical properties of the completed ingot. In recent years, related issues have been studied extensively, and comprehensive reviews have been published [1–4].

A common approach to predicting the behavior of a solidifying alloy uses a continuum formulation, which allows the entire domain to be modeled by one set of equations, thereby eliminating the need to explicitly track solidification fronts or to use artificial matching conditions at these fronts. In one approach, classical mixture theory is used to derive advection-diffusion equations which describe the transport of mixture mass, momentum, energy and species in terms of phase properties and phase mass fractions, thereby eliminating the need for detailed descriptions of phase interactions [5–8].

While continuum mixture models have enjoyed a measure of success in at least qualitatively predicting the behavior of solidifying ingots, the results are generally cast in terms of dimensional variables and are specific to the systems studied. The complex transport phenomena involved in a solidifying alloy usually require a full numerical solution to extract useful information from the equations. However, scaling principles [9, 10] can be applied to these equations to obtain useful results concerning the functional dependence of important macroscopic parameters on casting conditions and material properties. Scaling analysis can also be used to simplify systematically the governing equations by assessing the relative significance of the terms.

There have been few applications of these techniques to the full equations associated with solidification in a mushy layer. One recent application was concerned with developing a stability analysis and determining a critical Rayleigh number for the onset of convective flow [11]. However, a multidomain, rather than a continuum, formulation was used, with a prescribed interaction between the melt and mushy regions. It was also assumed, *a priori*, that D'Arcy's law with buoyancy applied to fluid flow everywhere in the two-phase region.

The only studies which apply scaling analysis to complete continuum mixture equations appear to be those by Amberg [12, 13], who considered an iron–carbon mixture solidified by imposing a constant and uniform heat flux at the side walls. The governing transport equations for a binary alloy were nondimensionalized, and order-of-magnitude estimates of various terms were used to derive a parameter map. In each parameter range, estimates were made of solidification time, degree of segregation, and mode of freezing. Also, the amount of undercooling in the bulk melt was determined and calculations were performed with the full equations to confirm the estimates.

The present work examines a bottom cooled binary alloy, modeled using the full continuum mixture model derived by Bennon and Incropera [6] and reassessed by Prescott *et al.* [8]. The transport equations are scaled in the mushy zone to provide order-of-magnitude estimates for streamfunctions and vel-

NOMENCLATURE

c	specific heat [J kg^{-1} K^{-1}]
D_l	liquid mass diffusion coefficient [m^2 s^{-1}]
Da	D'Arcy number, $K^{1/2}/\delta$
f	mass fraction
F	dimensionless composition
g	volume fraction; gravitational acceleration [m s^{-2}]
h	enthalpy [J]
h_f	heat of fusion [J kg^{-1}]
k	thermal conductivity [W m^{-1} K^{-1}]
K	permeability [m^2]
L	ingot height [m]
Nu	ingot Nusselt number, UL/k
P	pressure [N m^{-2}]
P_x, P_y	pressure gradients in x- and y-directions [N m^{-3}]
q''	heat flux [W m^{-2}]
$Ra_{K\delta}$	mushy zone Rayleigh number, $\rho g(\beta_S \Delta f^{\alpha}_{l,0} - \beta_T \Delta T_0) K\delta/(\mu\alpha)$
Re_K	mushy zone Reynolds number, $\rho_l v_0 K^{1/2}/\mu$
t	time [s]
T	temperature [K]
u	x-velocity [m s^{-1}]
U	overall heat transfer coefficient (W m^{-2} K^{-1})
v	y-velocity [m s^{-1}]
$\mathbf{V}$	velocity vector [m s^{-1}]
W	ingot width [m]
x, y	Cartesian coordinates [m].

Greek symbols

α	thermal diffusivity [m^2/s^{-1}]
β	contraction ratio
β_S	solutal expansion coefficient
β_T	thermal expansion coefficient [K^{-1}]
δ	mushy zone thickness [m]
δ_s	solid region thickness [m]
θ	dimensionless temperature
κ_0	permeability constant [m^2]
μ	dynamic viscosity [kg s^{-1} m^{-1}]
ρ	density [kg m^{-3}]
τ	dimensionless time
ψ	streamfunction [m^2 s^{-1}].

Subscripts

c	chill
i	initial
l	liquid
liq	liquidus
M	momentum
mp	melting point for pure component
0	reference value
s	solid
sol	solidus
T	thermal
w	bottom wall.

Superscripts

α	constituent of binary mixture
*	dimensionless variable.

ocities due to buoyancy effects, for mushy and solid layer thicknesses, and for chill wall temperature, and to show that certain terms in the momentum equations are negligible everywhere in the domain. Portions of the two-phase region in which convection has a significant effect on the transport of energy and species are also identified. Numerical calculations for Al–Mg and Pb–Sn systems, chilled from below over a range of thermal boundary conditions, are used to assess the results of the scaling analysis.

2. MATHEMATICAL FORMULATION AND NUMERICAL METHODS

Using the continuum mixture model for solidification of binary allows [6, 8], dimensional equations for the transport of mixture mass, momentum, enthalpy and species may be expressed as

$$\frac{\partial \rho}{\partial t} + \frac{\partial}{\partial x}(\rho u) + \frac{\partial}{\partial y}(\rho v) = 0 \quad (1)$$

$$\frac{\partial}{\partial t}(\rho u) + \nabla \cdot (\rho \mathbf{V} u) = \nabla \cdot \mu \frac{\rho}{\rho_l} \nabla u + \nabla \cdot \mu u \nabla\left(\frac{\rho}{\rho_l}\right) - \frac{\mu}{K_x}\frac{\rho}{\rho_l} u - \frac{\partial P}{\partial x} - \nabla \cdot \rho \frac{f_s}{f_l} \mathbf{V} u \quad (2)$$

$$\frac{\partial}{\partial t}(\rho v) + \nabla \cdot (\rho \mathbf{V} v) = \nabla \cdot \mu \frac{\rho}{\rho_l} \nabla v + \nabla \cdot \mu v \nabla\left(\frac{\rho}{\rho_l}\right) - \frac{\mu}{K_y}\frac{\rho}{\rho_l} v + \rho_l g(\beta_T(T - T_l) + \beta_S(f^{\alpha}_l - f^{\alpha}_{l,l})) - \frac{\partial P}{\partial y} - \nabla \cdot \rho \frac{f_s}{f_l} \mathbf{V} v \quad (3)$$

$$\frac{\partial}{\partial t}(\rho h) + \nabla \cdot (\rho \mathbf{V} h) = \nabla \cdot \left(\frac{k}{c} \nabla h\right) + \nabla \cdot \left(\frac{k}{c} \nabla (h_s - h)\right) - \nabla \cdot (\rho \mathbf{V}(h_l - h)) \quad (4)$$

$$\frac{\partial}{\partial t}(\rho f^{\alpha})+\nabla\cdot(\rho\mathbf{V}f^{\alpha})=\nabla\cdot(\rho f_{\mathrm{l}}D_{\mathrm{l}}\nabla f^{\alpha})$$

$$+\nabla\cdot(\rho f_{\mathrm{l}}D_{\mathrm{l}}\nabla(f_{\mathrm{l}}^{\alpha}-f^{\alpha}))-\nabla\cdot(\rho\mathbf{V}(f_{\mathrm{l}}^{\alpha}-f^{\alpha})). \quad (5)$$

The solid phase is assumed to be rigid and stationary, thereby eliminating several terms in the momentum equations of Prescott *et al.* [8]. Because recent experimental studies suggest that there is very little transport of free-floating solid particles in bottom cooled ingots [14], the assumption is believed to be valid for the conditions of this study. Another change in the momentum equations concerns relaxation of the assumption of equivalent solid and liquid densities. The second term on the right-hand side of equations (2) and (3) arises due to the difference in densities of the two phases. Although the last term on the right-hand side of equations (2) and (3) has been neglected previously [6, 8], it is retained temporarily in this study.

The permeability components, K_x and K_y, depend on the model linking microscopic drag effects to macroscopic flow. While the permeability of mushy zones is generally anisotropic, specific features are not well understood, and it is assumed that $K_x = K_y = K$. The permeability is evaluated from the Blake–Kozeny expression,

$$K=\kappa_0\frac{(1-g_s)^3}{g_s^2}, \quad (6)$$

where the permeability constants, κ_0, are based on representative dendritic arm spacings (DAS).

To assess results of the following scaling analysis, numerical studies were performed for a rectangular, bottom cooled ingot, with $W = 500$ mm and $L = 200$ mm (Fig. 1). In this mold, two different alloys, Al-14.9 wt%Mg and Pb-19.2 wt%Sn, were each chilled at two heat extraction rates until complete solidification was reached. Selection of the Al–Mg system was based on to its commercial significance, while Pb–Sn was chosen for its wide freezing range, which promotes macrosegregation. The dendritic arm spacing for Al–Mg was estimated to be 500 μm ($\kappa_0 = 1.4\times10^{-9}$ m^2), as suggested by photographs of dendrites [15] and, for Pb–Sn, the spacing was approximated as 71μm ($\kappa_0 = 2.8\times10^{-11}$ m^2) [16].

Initially, the alloys were assumed to be molten, quiescent and uniformly mixed, with temperatures exceeding the liquidus temperatures corresponding to the initial compositions by 5°C ($T_i = 287$°C for Pb–Sn, $T_i = 575$°C for Al–Mg). All walls were impermeable, with a no-slip condition. The top and side walls were insulated, while energy was extracted from the bottom at a rate governed by the instantaneous wall temperature, $T_w(t)$, and a uniform and constant overall heat transfer coefficient, U

$$q''(t) = U[T_w(t)-T_c]. \quad (7)$$

Values chosen for U in the lead–tin system were 1000 W m^{-2}K^{-1} and 10 000 W m^{-2} K^{-1}, while values

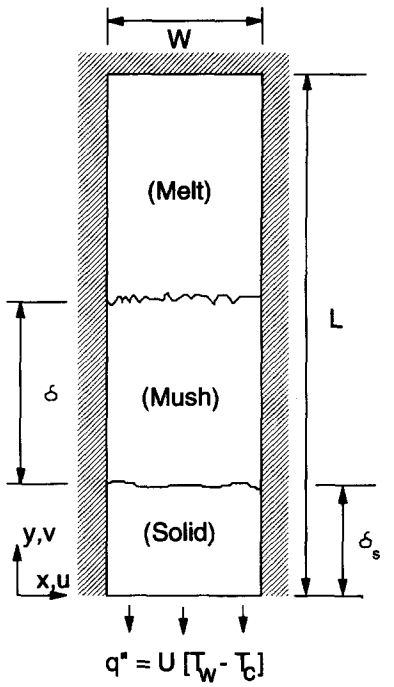

Fig. 1. System geometry.

for aluminum–magnesium were $U = 1000$ W m^{-2} K^{-1} and 2500 W m^{-2} K^{-1}. Selection of these values was dictated by the desire to maintain a liquid region above the mushy zone during much of the solidification process. If U is too small, a slow rate of solidification could cause the mush to fill the entire domain with small spatial variations of solid volume fraction and liquid composition. On the other hand, if U is too large, rapid solidification could preclude establishment of buoyancy induced flow, leaving little time for the weak diffusive or advective transport of solute. However, for extremely large solidification rates, solute may be transported by shrinkage driven flows, the effects of which are discussed elsewhere [17]. Hence, the overall heat transfer coefficients were selected to produce intermediate freezing range conditions.

The numerical scheme used to solve the conservation equations is SIMPLER, a control-volume-based finite difference method, with a fully implicit time marching technique [18]. The program uses a TDMA line-by-line solver with a block correction method, solving first for the pressure and velocity fields and then for the mixture enthalpy and composition. Using these mixture quantities, the lever law is applied to the linearized equilibrium phase diagrams, either for Pb–Sn or Al–Mg, to determine the local temperature, the fraction solid, and the composition of the solid and liquid phases. The expressions modeling the binary phase diagram are well documented [6, 19] and are not repeated here. The grid (85 × 50) provides a compromise between computational accuracy and speed and is comparable to that used in

previous simulations of lead–tin systems [17, 20]. The largest time steps which yielded quickly converged results varied with cooling rate, ranging from 1.0 to 0.01 s for slow and rapid cooling, respectively. These time steps were used at the beginning of solidification and increased as time progressed and the cooling rates decreased. Solutions were considered converged at a particular time step if they had residuals of mass, energy and species less than 10^{-4} for at least five consecutive iterations. The calculations were performed on HP-715 workstations and used approximately 250 CPU s per time step.

3. SCALING ANALYSIS

3.1. *Continuity and momentum equations*

The first step in scaling equations (1)–(3) is the *a priori* selection of reference values for as many variables as possible. These reference values should be chosen to give nondimensional variables of order unity. Because this study is primarily concerned with transport phenomena in the mushy zone, an obvious length scale for the vertical direction is the thickness of that zone, $y_0 = \delta (y^* = y/y_0)$. Emms and Fowler [9] show that, for bottom chilled solidification, the width of circulation cells transporting fluid between the mush and the melt is of the same order as the mushy zone thickness. Therefore, the horizontal length scale is equated to this thickness also, $x_0 = \delta$ $(x^* = x/x_0)$. Although this choice may be inappropriate if $\delta \gg W$, the mushy zone thickness does not exceed the order of the ingot width for the conditions of this study.

Initially, the density of each phase is assumed to be constant and uniform, with $\rho_s \neq \rho_l$. A dimensionless density which varies between zero and unity across the mush is defined as

$$\rho^* = \frac{\rho - \rho_l}{\rho_s - \rho_l} = \frac{\rho - \rho_l}{\beta \rho_l}, \tag{8}$$

where β is the contraction ration, $\beta = ((\rho_s - \rho_l)/\rho_l)$. Similarly, a dimensionless temperature and liquid composition can be expressed as

$$\theta = \frac{T - T_{liq}}{T_{sol} - T_{liq}} = \frac{T - T_{liq}}{\Delta T_0} \tag{9}$$

and

$$F_l = \frac{f_l^\alpha - f_{l,i}^\alpha}{f_{l,sol}^\alpha - f_{l,i}^\alpha} = \frac{f_l^\alpha - f_{l,i}^\alpha}{\Delta f_{l,0}^\alpha}. \tag{10}$$

The temperatures T_{liq} and T_{sol} correspond to the liquidus and solidus temperatures at the initial composition, $f_{l,i}^\alpha$. The maximum liquid composition, $f_{l,sol}^\alpha$, exists when the last liquid freezes at $T = T_{sol}$.

As a time scale, Emms and Flower [11] and Amberg [13] chose $t_{0,M} = L^2/\alpha$, which is a measure of the time required for heat to diffuse the distance L. However, while convenient for purposes of nondimensionalization, this choice is not a physically appropriate reference for the momentum equations. A more appropriate scale is the time required for liquid to be advected across the distance y_0, or $t_{0,M} \sim \delta/v_0$, where v_0 is an appropriate vertical velocity scale.

Recasting the continuity equation (1) in terms of scaled quantities,

$$\frac{\partial(\rho^*\beta + 1)}{\partial t^*} + \left(\frac{u_0}{v_0}\right)\frac{\partial(\rho^*\beta + 1)u^*}{\partial x^*} + \frac{\partial(\rho^*\beta + 1)v^*}{\partial y^*} = 0. \tag{11}$$

Because the contraction ratio, β, is in the range from 2 to 12% for metal systems, the last two terms on the left-hand side of equation (11) are the same order of magnitude,

$$\left(\frac{u_0}{v_0}\right)\frac{\partial u^*}{\partial x^*} \sim \frac{\partial v^*}{\partial y^*}, \tag{12}$$

in which case, $u_0 \sim v_0$.

Using the foregoing reference values, the vertical momentum equation (3) may be nondimensionalized with the D'Arcy drag term assumed to be important throughout the mushy zone. Rearranging the dimensionless equation to yield a coefficient of unity for the D'Arcy term, it follows that

$$\begin{aligned} Re_K Da\left[\frac{\partial v^*}{\partial t^*} + u^*\frac{\partial v^*}{\partial x^*} + v^*\frac{\partial v^*}{\partial y^*} + \nabla^* \cdot \frac{f_s}{f_l}\frac{\mathbf{V}^* v^*}{(\rho^*\beta + 1)}\right] \\ = Da^2\left[\nabla^{*2} v^* + \frac{\beta}{\rho^*\beta + 1}\left(2\frac{\partial \rho^*}{\partial x^*}\frac{\partial v^*}{\partial x^*} + 2\frac{\partial \rho^*}{\partial y^*}\frac{\partial v^*}{\partial y^*}\right.\right. \\ \left.\left. + v^*\nabla^{*2}\rho^*\right)\right] - v^* - \left(\frac{P_{y0}K}{\mu(\rho^*\beta + 1)v_0}\right)\frac{\partial P^*}{\partial y^*} \\ + \left(\frac{\rho_l g \beta_T \Delta T_0 K}{(\rho^*\beta + 1)\mu v_0}\right)\theta + \left(\frac{\rho_l g \beta_S \Delta f_{l,0}^\alpha K}{(\rho^*\beta + 1)\mu v_0}\right)F_l, \end{aligned} \tag{13}$$

where $Re_K = \rho_l v_0 K^{1/2}/\mu$, $Da^2 = K/\delta^2$ and P_{y0} is a reference for the vertical pressure gradient.

Before estimating values of the coefficients in equations (13), the second, third and fourth terms within the bracketed quantity on the right-hand side, which represent viscous stresses arising from density variations, are examined. Because $\beta \ll 1$, $\beta/(\rho^*\beta + 1) \ll 1$, and these three terms are negligible everywhere compared to the remaining viscous term, $\nabla^{*2} v^*$. Hence, the terms can be neglected. Moreover, because the remaining term is of order Da^2, its influence inside the mushy zone is limited to regions near the liquidus interface. Considering a mushy zone thickness of $\delta = 10$ mm as an example, $Da^2 \ll 1$ for $g_s \gtrsim 0.005$ in the Pb–Sn system and for $g_s \gtrsim 0.02$ in the Al–Mg system. Because the calculations described in Section 2 show that $\delta = 10$ mm is relatively small for all but the highest freezing rates, it is reasonable to neglect all viscous terms inside the mushy zone.

The left-hand side of equation (13) is of order $Re_K Da$. With the numerical calculations yielding velocities near the liquidus line of approximately 10^{-3} m

s^{-1} for Pb–Sn and 10^{-2} m s^{-1} for Al–Mg, and assuming a mushy layer thickness of $\delta = 10$ mm, all terms on the left-hand side are negligible for $g_s \gtrsim 0.01$ and $g_s \gtrsim 0.1$ in the Pb–Sn and Al–Mg systems, respectively. For this reason, penetration of advective effects into the mush often is neglected in multidomain models [e.g. 11, 21], and flow in the two-phase region is determined only from D'Arcy's law and continuity. However, because channel initiation and growth appear to be strongly affected by the transport of solute near the liquidus interface [22, 23], the advective effects should be retained in studies of channel and freckle development.

While the left-hand side of equation (13) is significant only in the regions of the mushy zone near the liquidus isotherm, the first three terms remain important throughout the adjoining bulk liquid region. The last term is identically zero in the bulk liquid, and, because it is of order $Re_K Da(f_s/f_l)$ in the mush, where $(f_s/f_l) \Rightarrow 0$ near the liquidus, it is negligible in this region also. Hence, as done in prior studies [6, 8], the term can be neglected everywhere throughout the mushy and liquid regions. The foregoing order-of-magnitude analysis yields a reduced continuum momentum equation which has the dimensional form

$$\frac{\partial}{\partial t}(\rho v)+\nabla\cdot(\rho \mathbf{V} v) = \nabla\cdot\mu\nabla v-\frac{\mu}{K}v + \rho g(\beta_T(T-T_i)+\beta_S(f_l^{\alpha}-f_{l,i}^{\alpha}))-\frac{\partial P}{\partial y}. \quad (14)$$

Neglecting terms which are estimated to be small in most of the mushy zone, and again using $\rho^*\beta \ll 1$, equation (13) reduces in that region to

$$0 \approx -v^*-\left(\frac{P_{y0}K}{\mu v_0}\right)\frac{\partial P^*}{\partial y^*}+\left(\frac{\rho g\beta_T\Delta T_0 K}{\mu v_0}\right)\theta + \left(\frac{\rho g\beta_S\Delta f_{l,0}^{\alpha}K}{\mu v_0}\right)F_{l^*}. \quad (15)$$

Assuming that the mixture composition does not vary significantly from the original composition, the temperature and liquid composition are linked through the phase diagram. Approximating the liquidus line on the eutectic phase diagram as linear, the definitions for dimensionless temperature and liquid composition give $\theta = -F_l$ and equation (15) can be written as

$$0 \approx -v^*-\left(\frac{P_{y0}K}{\mu v_0}\right)\frac{\partial P^*}{\partial y^*}+\left(\frac{\rho g(\beta_S\Delta f_{l,0}^{\alpha}-\beta_T\Delta T_0)K}{\mu v_0}\right)F_l. \quad (16)$$

A similar relation can be found for the x momentum equation (2).

$$0 \approx -u^*-\left(\frac{P_{x0}K}{\mu v_0}\right)\frac{\partial P^*}{\partial x^*}. \quad (17)$$

Assuming that $P_{x0} \sim P_{y0}$, differentiating equations (16) and (17) with respect to x and y, respectively, and subtracting one from the other, it follows that,

$$\frac{\partial v^*}{\partial x^*}-\frac{\partial u^*}{\partial y^*} \approx \left(\frac{\rho g(\beta_S\Delta f_{l,0}^{\alpha}-\beta_T\Delta T_0)K}{\mu v_0}\right)\frac{\partial F_l}{\partial x^*}. \quad (18)$$

Rewriting equation (18) in terms of a streamfunction, ψ, where $u = \partial\psi/\partial y$ and $v = -\partial\psi/\partial x$, and using $\psi_0 \approx v_0\,\delta$ to scale ψ, it follows that

$$-\nabla^2\psi^* \approx \left(\frac{\rho g(\beta_S\Delta f_{l,0}^{\alpha}-\beta_T\Delta T_0)K\delta}{\mu\psi_0}\right)\frac{\partial F_l}{\partial x^*}, \quad (19)$$

where $\psi^* = \psi/\psi_0$. This result leads to the following scaling laws for the streamfunction,

$$\psi_0/\alpha \sim \frac{\rho g(\beta_S\Delta f_{l,0}^{\alpha}-\beta_T\Delta T_0)K\delta}{\mu\alpha} = (Ra)_{K\delta}, \quad (20)$$

and the velocity,

$$v_0 \sim \frac{\rho g(\beta_S\Delta f_{l,0}^{\alpha}-\beta_T\Delta T_0)K}{\mu}. \quad (21)$$

Equation (21), which gives the reference velocity as a function of K and, therefore, g_s, is suitable for estimating velocity variations in the mushy zone. Also, as will be shown below, it is useful for determining regions in which advection can significantly affect energy and species transfer.

3.2. *Energy equation*

Although the dimensional energy equation (4) has been written in the form of an advection–diffusion equation which is convenient for numerical calculations, an alternative formulation is better suited for the scaling analysis. In particular, equation (4) may be expressed as

$$\frac{\partial(\rho h)}{\partial t}+\nabla\cdot(\rho\mathbf{V}h_l) = \nabla\cdot\left(\frac{k}{c}\nabla h_s\right). \quad (22)$$

Scaling the solid, liquid and mixture enthalpies such that the nondimensional quantities vary from zero at the solidus to unity at the liquidus, it follows that

$$h_s^* = \frac{h_s-cT_{sol}}{c(T_{liq}-T_{sol})} = \frac{h_s-cT_{sol}}{c\Delta T_0}, \quad (23)$$

$$h_l^* = \frac{h_l-(cT_{sol}+h_f)}{c\Delta T_0}, \quad (24)$$

and

$$h^* = \frac{h-cT_{sol}}{\Delta h}, \quad (25)$$

where $\Delta h \equiv c\Delta T_0 + h_f$. Accordingly, substituting from equations (8) and (25), nondimensionalization of the transient term yields

$$\frac{\partial(\rho h)}{\partial t} = \frac{\rho_l}{t_{0,T}}\left[(\beta\Delta h)\frac{\partial(\rho^* h^*)}{\partial t^*} + (\beta c T_{sol})\frac{\partial \rho^*}{\partial t^*} + \Delta h \frac{\partial h^*}{\partial t^*}\right] \tag{26}$$

or, with $\beta \ll 1$,

$$\frac{\partial(\rho h)}{\partial t} \sim \frac{\rho_l \Delta h}{t_{0,T}}\frac{\partial h^*}{\partial t^*}. \tag{27}$$

Substituting from equations (23)–(25) and (27), the scaled form of the energy equation (22) is

$$\frac{\partial h^*}{\partial t^*} + \left(\frac{c v_0}{k}\frac{t_{0,T} k \Delta T_0}{\Delta h \delta}\right)\left[u^*\frac{\partial h_l^*}{\partial x^*} + v^*\frac{\partial h_l^*}{\partial y^*}\right] \sim \left(\frac{t_{0,T} k \Delta T_0}{\rho \Delta h \delta^2}\right)\frac{\partial^2 h_s^*}{\partial y^{*2}}, \tag{28}$$

where the prescription of adiabatic side walls is presumed to render diffusion in the x-direction negligible.

The results of numerical calculations indicate that the temperature field in bottom chilled ingots depends on y and x near the liquidus and in the melt. Because of the time dependent nature of this problem, the transient term is always significant and is balanced by a combination of advective and diffusive effects. Estimates of the ratio of the advective and diffusive coefficients in equation (28), assuming that the unknown proportionality constant in equation (21) is approximately unity, indicate that the ratio is larger than order unity for $g_s \leqslant 0.15$ and $g_s \leqslant 0.25$ in the Pb–Sn and Al–Mg systems, respectively, demonstrating that advective effects do indeed dominate near the liquidus line. In the remainder of the mushy zone, however, the advective term is, *at most*, of order unity.

In order to obtain order-of-magnitude estimates for the mushy zone and solid region thicknesses and the chill wall temperature, the freezing of the alloy is divided into two temporal regimes: (i) $T_w > T_{sol}$, in which the mushy zone is in contact with the chill wall and no region of the domain is completely solid, and (ii) $T_w \leqslant T_{sol}$, in which totally solid region exists between the chill wall and the mush (see Fig. 1). Considering the first regime and neglecting advection throughout the mushy zone, the energy equation can be approximated by

$$\frac{1}{\alpha}\frac{\partial T}{\partial t} - \frac{\rho h_f}{k}\frac{\partial f_s}{\partial t} = \frac{\partial^2 T}{\partial y^2}, \tag{29}$$

which is subject to the conditions,

$$k\left.\frac{\partial T}{\partial y}\right|_{y=0} = U(T_w(t) - T_c) \tag{30}$$

and

$$T(t=0) \approx T_{liq}. \tag{31}$$

This last condition holds if the superheat is small compared to the temperature across the mushy zone.

Using the chain rule, equation (29) can be rewritten as

$$\left(\frac{1}{\alpha} - \frac{\rho h_f}{k}\frac{\partial f_s}{\partial T}\right)\frac{\partial T}{\partial t} = \frac{\partial^2 T}{\partial x^2}, \tag{32}$$

where [19]

$$f_s(T) = \frac{1}{1-k_p}\left(\frac{T - T_{liq}}{T - T_{mp}}\right). \tag{33}$$

Equation (32) can be scaled, yielding

$$\left[1 + \left(\frac{h_f}{c\Delta T_0}\right)\left(\frac{1}{1-k_p}\right)\left(\frac{\theta_{mp} - \theta_{liq}}{(\theta - \theta_{mp})^2}\right)\right] \times \frac{1}{\alpha}\frac{(T_{liq} - T_w)}{t} \sim \frac{(T_{liq} - T_w)}{\delta^2}, \tag{34}$$

where $\theta = (T - T_c)/(T_{liq} - T_{sol})$. Because the second term in the transient coefficient is generally order unity for the metal systems examined here, it follows that

$$\delta^* \sim \tau^{1/2}, \tag{35}$$

where $\delta^* = \delta/L$ and $\tau = t\alpha/L^2$. This relation holds even after the solid region forms at the chill surface.

Replacing $(T_{liq} - T_w)$ by $(T_{liq} - T_{sol})$, the foregoing analysis may be repeated for the conditions following formation of a solid region. With energy transfer in the solid occurring exclusively by conduction, the thickness of the solid layer may be scaled as

$$\delta_s^* \sim \tau_s^{1/2}, \tag{36}$$

where $\delta_s^* = \delta_s/L$, $\tau_s = (t - t_{sol})\,\alpha/L^2$ and t_{sol} is the time at which $T_w = T_{sol}$.

To understand the transient behavior of the chill wall temperature, equation (30) is scaled as

$$k\frac{T_\chi - T_w}{\delta_\chi} \sim U(T_w - T_c), \tag{37}$$

where conditions associated with the subscript χ depend on the temporal regime. While the mushy zone is in contact with the chill wall, $T_\chi = T_{liq}$ and $\delta_\chi = \delta$. After the completely solid region begins to form, $T_\chi = T_{sol}$ and $\delta_\chi = \delta_s$. Rearranging and nondimensionalizing equation (37) it follows that, for $Nu = UL/k$,

$$\theta_w \sim \frac{\theta_{liq}}{1 + Nu\delta^*} \tag{38}$$

for the first regime and

$$\theta_w \sim \frac{\theta_{sol}}{1 + Nu\delta_s^*} \tag{39}$$

after the solid region forms. Equating these two relations at the time the completely solid region begins to form (τ_{sol}), when $\delta_s = 0$, the following scaling law is obtained:

$$\tau_{sol} \sim \left[\frac{1}{Nu}\left(\frac{\theta_{liq}}{\theta_{sol}} - 1\right)\right]^2. \quad (40)$$

3.3. *Species equation*

Reducing equation (5) to a form which is better suited for scaling and substituting from equation (10), the scaled solute transport equation may be expressed as

$$\frac{\partial F}{\partial t^*} + \left(\frac{t_{0,s} v_0}{\delta}\right)\left[u^* \frac{\partial F_l}{\partial x^*} + v^* \frac{\partial F_l}{\partial y^*}\right] = \left(\frac{t_{0,s}(\rho^* \beta + 1) f_l D_l}{\delta^2}\right)\frac{\partial^2 F_l}{\partial y^{*2}}. \quad (41)$$

Using this equation, the transport mechanism which dominates changes in mixture composition can be determined. From equation (41), the ratio of coefficients associated with transport due to advection and diffusion is $\delta\, v_0/(\rho^* \beta + 1)\, f_l\, D_l$. Calculations of this quantity for the conditions of this study show that advection dominates species transport for the entire mushy zone. The diffusion coefficient is small, $D_l \sim 10^{-9}$, and although liquid velocities are very small deep within the mushy zone, advection remains the dominant transport mode.

3.4. *Summary of scaling analysis*

Scaling of the conservation equations has provided new insights concerning transport of momentum, energy and species in a mushy zone. The resulting velocity and streamfunction scales show the dependence on fluid properties, buoyancy, and the local permeability of the mushy zone. From the energy equation, scaling laws for the thicknesses of the two-phase and solid regions and for the chill wall temperature have been obtained. Estimates of the extent of penetration of significant advective effects into the mushy zone for the momentum and energy equations have shown that such effects are dominant only near the liquidus. However, scaling of the species equation indicates that solute transport is driven by liquid motion throughout the entire mushy zone.

4. ASSESSMENT OF SCALING ANALYSIS

Calculations were performed to assess the results of the scaling analysis, with two cooling rates considered for each of the two alloys. Streamfunctions, velocities, mushy and solid region thicknesses, and chill wall temperatures were computed from detailed numerical simulations and the trends were compared to the scaling relations found in the previous section.

The first scaling relationship that is tested quantitatively is that for the streamfunction, equation (20). A plot of a typical streamfunction pattern (Al–Mg, $U = 1000$ W m^{-2} K^{-1}, $t = 80$ s) is shown in Fig. 2. This pattern is representative of conditions after significant flows are established in the mushy zone and before the top of the computational domain begins to affect the flow patterns. In Fig. 2, the streamlines indicate the presence of two regions of upflow (channels, or freckles) along the side walls, with an area of downflow in the center.

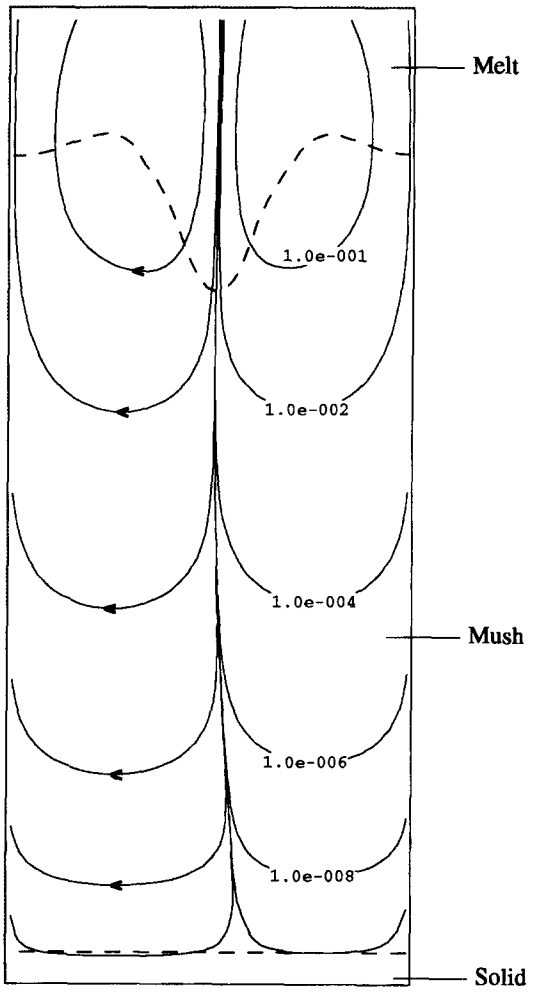

Fig. 2. Representative streamfunction pattern in mushy zone (Al–Mg, $U = 1000$ W m^{-2} K^{-1}, $t = 80$ s).

The maximum value of ψ/α at each discrete y location in the computational domain is plotted against corresponding values of $Ra_{K\delta}$ in Fig. 3 for some representative times for each of the four casting conditions. For the Al–Mg ingot, results are shown at $t = 100$ and 300 s for the low cooling rates and $t = 100$ s for the higher rate. For the Pb–Sn system, results correspond to $t = 500$ for both cases. The results show that the mushy zone Rayleigh number correctly represents the dependence of maximum streamfunction on material properties, solid volume fraction and mushy zone thickness. The dependence breaks down near the liquidus (large $Ra_{K\delta}$), where advective effects become important, and near the solidus ($Ra_{K\delta} \Rightarrow 0$), where the solid region stops all flow. Flow into a

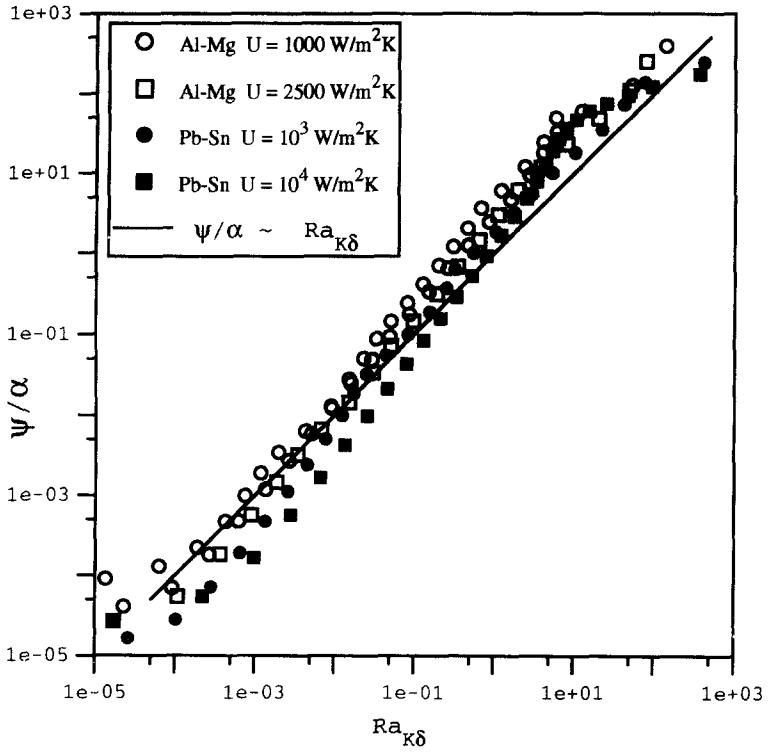

Fig. 3. Calculated maximum streamfunction values as a function of corresponding mushy zone Rayleigh number.

channel is dominated by fluid which enters from regions near the liquidus line, with inflow from locations deeper in the mush making almost no contribution to the total mass flow through the channel. (The difference between the values of ψ defining any two streamlines is the volume flow rate between those two streamlines [24] and, hence, corresponds to the amount of liquid entrained into the channels from the mushy zone.) This result leads to the conclusion that the composition of the plumes ejected into the bulk melt from the channels should be closer to the initial value than to the liquid composition near the solidus front. This conclusion agrees with the experimental observations of Hellawell *et al.* [25], who measured the composition of plumes in NH_4Cl–H_2O systems during freezing and of channels in solidified Pb–Sb alloys and deduced that most of the flow entrained into the channels from the mushy zone is from the near-liquidus region.

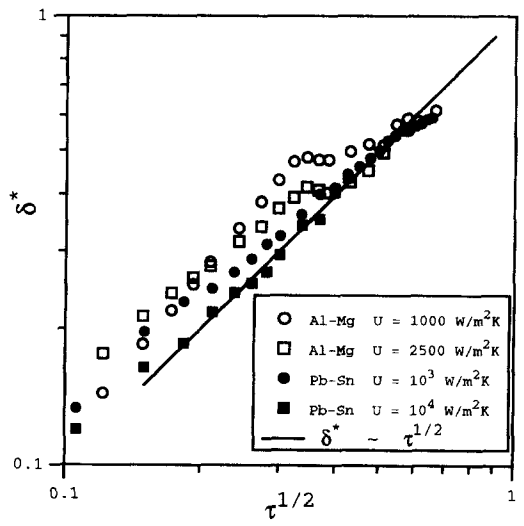

Fig. 4. Dimensionless mushy zone thicknesses as a function of dimensionless time.

In Fig. 4, numerical results for the dimensionless mushy zone thickness are plotted as a function of $\tau^{1/2}$ to assess the validity of the scaling relation given by equation (35). The predictions agree well with the $\tau^{1/2}$ dependence suggested by the approximate analysis, until later stages of solidification when the liquidus isotherm approaches the top of the numerical domain. By this time, the lighter component (tin or magnesium) rejected from the mushy zone accumulates in the top of the cavity. This solute rich region has a lower liquidus temperature than the initial composition (assumed in the scaling analysis), which retards the growth of the mushy zone. The numerical results in Fig. 5, which illustrate the dependence of the solid region thickness on time, equation (36), do not exhibit significant changes in slope at larger values of τ, because the upper boundary of this region is always at T_{sol}, which, for the conditions of this study, does not change significantly. The curves have different intercepts to the $\delta_s^* = 0$ line because the four cases begin forming a totally solid region at different times. The foregoing trends are consistent with measure-

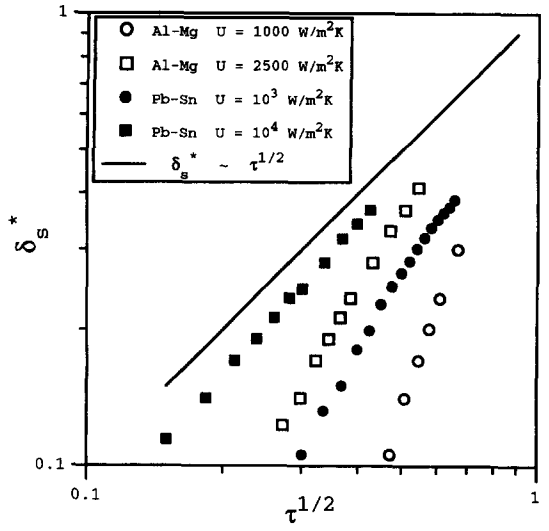

Fig. 5. Dimensionless solid region thicknesses as a function of dimensionless time.

ments of the mushy and solid region thicknesses made for a side-cooled Al–Cu alloy at two different compositions [26], where both δ and δ_s were found to depend on $t^{1/2}$

The numerical simulations were used to obtain the maximum velocity and the corresponding local solid volume fraction at each discrete y location in the mushy zone and at selected times until the mushy zone approached the top of the computational domain. The velocities are plotted for the Al–Mg (Fig. 6) and Pb–Sn (Fig. 7) systems as a function of solid volume fraction, along with a curve which is proportional to the reference velocity found by the scaling analysis in equation (21). In Fig. 6, velocities correspond to $U = 1000$ W m^{-2} K^{-1} for $100 \leqslant t \leqslant 300$ s and $U = 2500$ W m^{-2} K^{-1} for $80 \leqslant t \leqslant 200$ s. Figure 7 provides velocities for $75 \leqslant t \leqslant 700$ s for both $U = 1000$ W m^{-2} K^{-1} and for $U = 10\,000$ W m^{-2} K^{-1}.

The scaling analysis predicted that v_0 is independent of cooling rate, and, for a given alloy, depends only on the solid volume fraction. The numerical results show little or no dependence on cooling rate, and, with one exception, consistent trends are predicted for the dependence on solid volume fraction. The exception pertains to the Al–Mg system (Fig. 6) for small values of g_s. The velocity dependence of equation (21) is based on a balance between the buoyancy and drag forces imposed by the dendritic matrix. Estimates of the orders of magnitude of the terms in equation (13) suggest that advection and, to a lesser degree, viscous forces become important near the liquidus line ($g_s = 0$). The estimates also suggest that penetration of these effects into the mushy zone is larger for the Al–Mg system than for Pb–Sn. For the lead–tin alloy, the buoyancy-D'Arcy drag force balance is valid for practically the entire mush, while buoyancy driven flows in the Al–Mg system are restrained near the liquidus ($g_s < 0.05$) by the other effects. This difference explains the departure of the numerically predicted velocities from the trend shown by the scaling relation in Fig. 6, while such a departure is not prominent in Fig. 7.

The scaling analysis was also used to predict the dependence of the transient chill wall temperature on the casting conditions, and the results were compared to those obtained numerically. Figure 8 shows the wall temperature, θ_w, taken from equation (38) for the period during which the mush contacts the chill wall ($T_w > T_{sol}$). For the Al–Mg cases, the scaling law is only approximately representative at short times (high θ_w), when there is a very small mushy zone and the

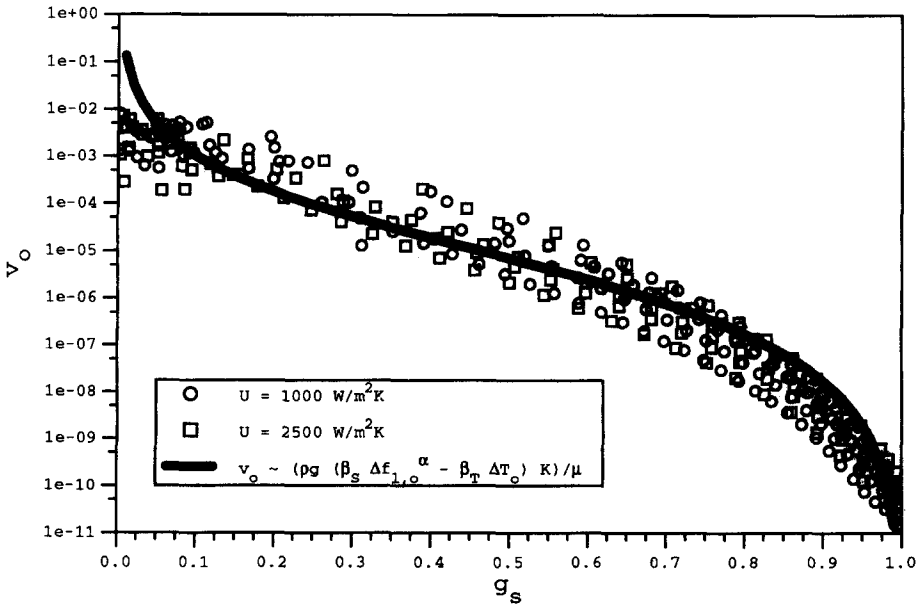

Fig. 6. Comparisons of scaling relations with predicted maximum mushy zone velocity for the Al–Mg system.

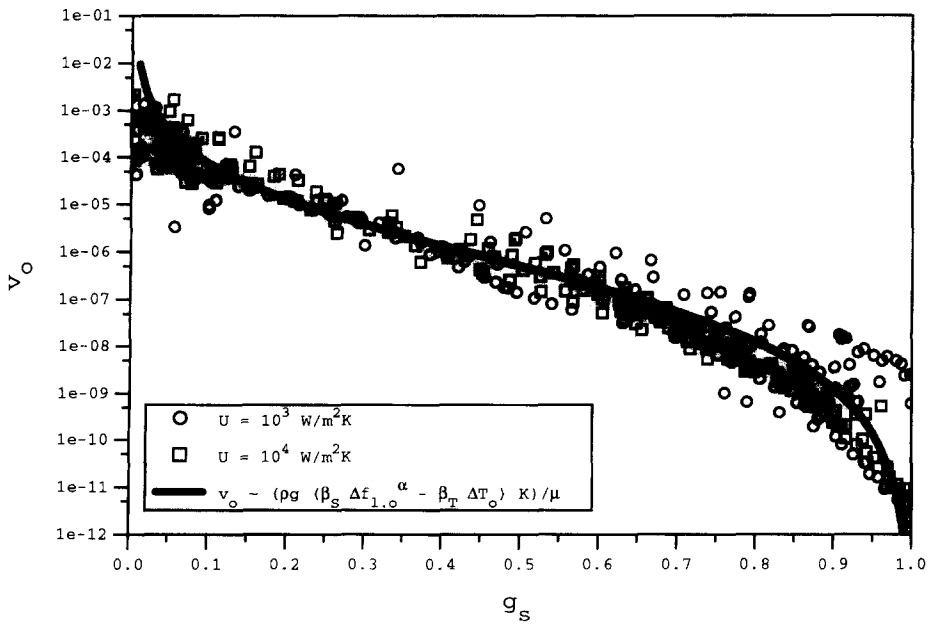

Fig. 7. Comparisons of scaling relations with predicted maximum mushy zone velocity for the Pb–Sn system.

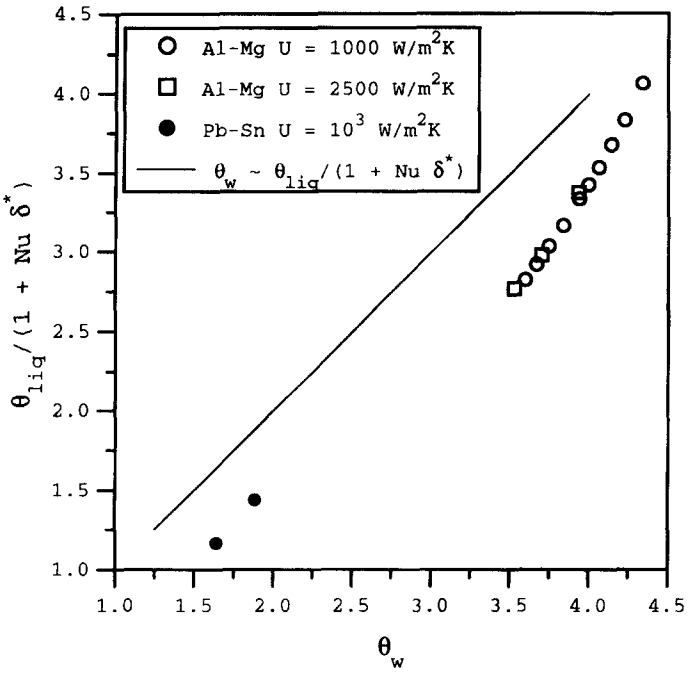

Fig. 8. Comparison of chill wall temperatures obtained from numerical predictions and scaling analysis ($\tau < \tau_{sol}$).

contribution of latent heat release is important. At later times, and in the low U Pb–Sn case, the proportionality predicted by the scaling analysis matches the numerical results very well. The high cooling rate case for Pb–Sn is not plotted because a solid region forms almost immediately. After the time at which solid formed at the chill surface, the scaling analysis, equation (39), is in excellent agreement with the numerical solution for the chill wall temperature (Fig. 9). The dependence associated with the scaling law for the time at which solid begins to form at the chill surface, equation (40), is compared to and exhibits excellent agreement with the numerical results (Fig. 10).

Scaling of the species transport equation showed that advection dominates the redistribution of solute throughout most of the mushy zone. Although this result might imply that the mixture composition of

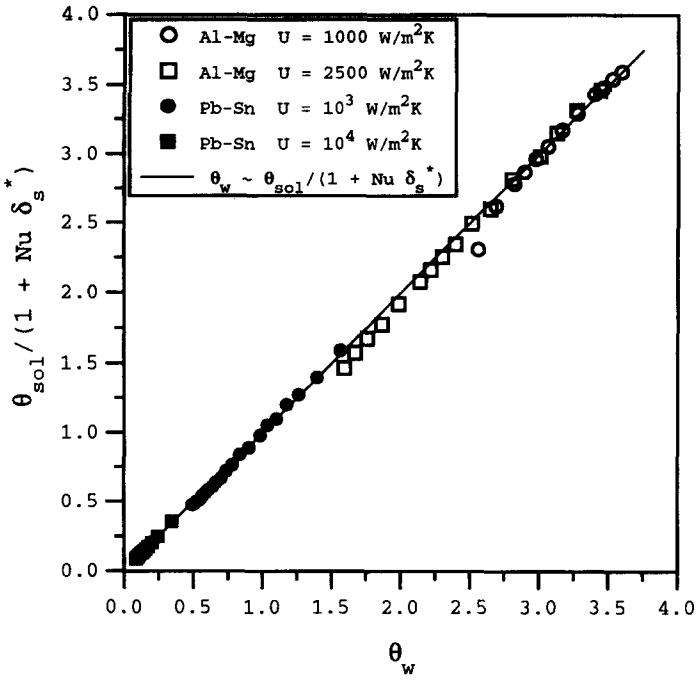

Fig. 9. Comparison of chill wall temperatures obtained from numerical predictions and scaling analysis ($\tau \geqslant \tau_{sol}$).

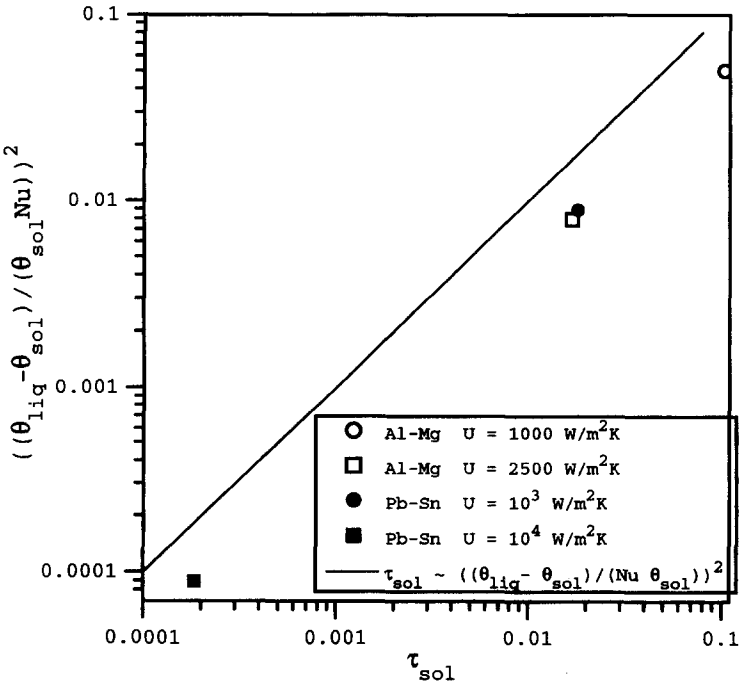

Fig. 10. Time at which solid region begins to form at chill surface.

the mushy layer should change considerably over time, Fig. 11, which presents centerline mixture compositions for the Pb–Sn and Al–Mg alloys at $U = 10^4$ W m^{-2} K^{-1} and $U = 2500$ W m^{-2} K^{-1}, respectively, suggests a different conclusion. Figure 11(a) compares composition profiles at 250 s and at a later time (1150 s) for which material within the two-phase region at 250 s is completely solidified. In the intervening 900 s, only a region very close to the liquidus has undergone further redistribution of solute, while most of the mush remains unaffected. Figure 11(b) shows Al–Mg centerline profiles at 90 and 300 s. Over this 210 s period, there is some change in the composition over the upper half of the mushy zone and a significant change in the upper quarter of the zone. In denser regions of the mush, liquid velocities are too slow to

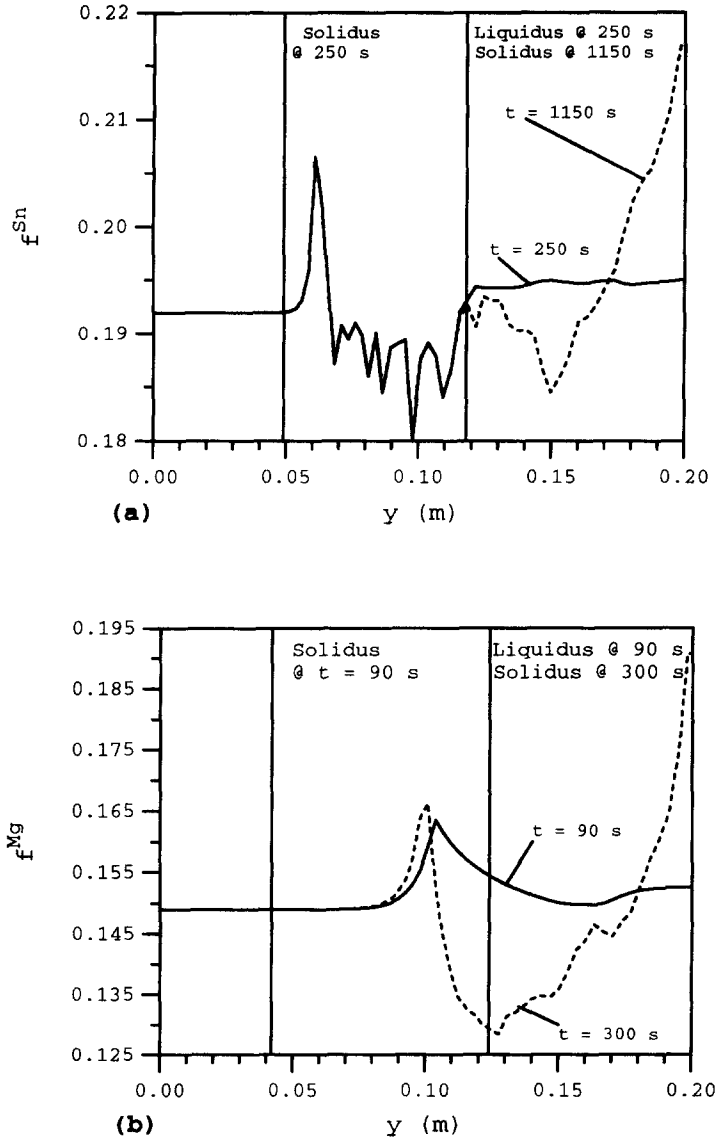

Fig. 11. Centerline composition profiles: (a) Pb–Sn for $U = 10^4$ W m^{-2} K^{-1} at $t = 250$ s and $t = 1150$ s; (b) Al–Mg for $U = 2500$ W m^{-2} K^{-1} at $t = 90$ s and $t = 300$ s.

significantly influence solute redistribution by advection before complete solidification occurs. The difference between the two cases is reconciled by the scaling analysis, which predicts deeper penetration of advective effects into the mushy zone for Al–Mg than for Pb–Sn. This deeper penetration is due primarily to the more permeable mushy zone of the Al–Mg system. Therefore, although the scaling analysis reveals that solute movement is dominated by advection, the numerical predictions show that the mixture composition in the mushy zone is only affected near the liquidus.

5. SUMMARY

A set of continuum mixture equations for mass, momentum, energy and species transport has been nondimensionalized by introducing physically meaningful scales, and a scaling analysis has been performed. This analysis has been evaluated quantitatively by comparing results with those obtained from detailed numerical calculations for two metal alloys convectively cooled from below. Treatment of the momentum equations, which yielded estimates for the streamfunction and buoyancy driven velocity in the mushy zone, indicated that D'Arcy's law provides a reasonable approximation for momentum transport in regions for which $Re_K Da \ll 1$. Several terms in these equations were found to be negligible in all regions of a solidifying ingot and a momentum equation retaining only significant effects was developed. Consistent trends were found between velocities and streamfunctions calculated from the scaling analysis and the numerical simulation.

The energy equation yielded scaling laws for the mushy zone and solid region thicknesses, as well as the transient chill wall temperature, which are consistent with trends numerically calculated using the full equations. The effect of cooling conditions and the alloy phase diagram on the time required for initiation of a fully solid region was also predicted accurately. Although the scaling analysis indicated that species transport was dominated by the advection of liquid throughout the two phase region, the numerical predictions showed that velocities were too small for liquid motion to affect macrosegregation patterns of the denser regions of the mushy layer before complete solidification occurred.

Acknowledgements—The authors would like to thank the Department of Energy for support of this research through award number DE-FG02-87ER13759. The first author would also like to acknowledge Dr R.J. Krane and Mr J.C. Rozzi for many useful discussions during the course of this work.

REFERENCES

1. R. Viskanta, Mathematical modeling of transport process during solidification of binary systems, *JSME Int. J. Ser.* II. **33,** 409–423 (1990).
2. C. Beckermann and R. Viskanta, Mathematical modeling of transport phenomena during alloy solidification, *Appl. Mech. Rev.* **46,** 1–27 (1993).
3. P. J. Prescott and F. P. Incropera, Binary solid–liquid phase change with fluid flow. In *Advances in Transport Processes* (Edited by A. S. Mujumdar and R. A. Mashelkar), Vol. IX. Elsevier, Amsterdam (1993).
4. P. J. Prescott and F. P. Incropera, Convection heat and mass transfer in alloy solidification. In *Advances in Heat Transfer*. Academic Press, New York (in press).
5. V. P. Voller and C. Prakash, A fixed-grid numerical modelling methodology for convection–diffusion mushy region phase-change problems, *Int. J. Heat Mass Transfer* **30,** 1709–1719 (1987).
6. W. D. Bennon and F. P. Incropera, A continuum model for momentum, heat and species transport in binary solid–liquid phase change systems—I. Model formulation, *Int. J. Heat Mass Transfer* **30,** 2161–2170 (1987).
7. G. Amberg, Computation of macrosegregation in an iron–carbon cast, *Int. J. Heat Mass Transfer* **34,** 217–227 (1991).
8. P. J. Prescott, F. P. Incropera and W. D. Bennon, Modelling of dendritic solidification systems: reassessment of the continuum momentum equation, *Int. J. Heat Mass Transfer* **34,** 2351–2359 (1991).
9. A. Bejan, *Heat Transfer*. Wiley, New York (1993).
10. A. Bejan, *Convective Heat Transfer* (2nd Edn). Wiley, New York (1994).
11. P. W. Emms and A. C. Fowler, Compositional convection in the solidification of binary alloys, *J. Fluid Mech.* **262,** 111–139 (1994).
12. G. Amberg, Scale analysis and numerical simulation of solidification of an alloy cooled at a vertical boundary. In *Interactive Dynamics of Convection and Solidification* (Edited by S. H. Davis, H. E. Huppert, U. Müller and M. G. Worster). Kluwer, Amsterdam (1992).
13. G. Amberg, Derivation of parameter ranges in binary solidification, TRITA-MEK TR 1993:9, Department of Mechanics, The Royal Institute of Technology, Stockholm, Sweden (1993).
14. W. C. Montgomery, Fragmentation and remelting of dendritic crystals associated with the solidification of aqueous ammonium chloride, M.S. thesis, School of Mechanical Engineering, Purdue University, West Lafayette, Indiana (1996).
15. W. Bingbo, Unidirectional dendritic solidification under longitudinal resonant vibration, *Acta Metall. Mater.* **40,** 2739–2751 (1992).
16. R. Nasser-Rafi, R. Deshmukh and D. R. Poirier, Flow of interdendritic liquid and permeability in Pb-20 wt pct Sn alloys, *Met. Trans. A* **16A,** 2263–2271 (1985).
17. M. J. M. Krane and F. P. Incropera, Analysis of the effect of shrinkage on macrosegregation in alloy solidification, *Met. Mater. Trans. A* **26A,** 2329–2339 (1995).
18. S. Patankar, *Numerical Heat Transfer and Fluid Flow*. Hemisphere, New York (1980).
19. W. D. Bennon and F. P. Incropera, Numerical analysis of binary solid–liquid phase change using a continuum model, *Numer. Heat Transfer* **13,** 277–296 (1988).
20. P. J. Prescott and F. P. Incropera, Convective transport phenomena and macrosegregation during solidification of a binary metal alloy: I—numerical predictions, *J. Heat Transfer* **116,** 735–741 (1994).
21. M. G. Worster, Natural convection in a mushy layer, *J. Fluid Mech.* **224,** 335–359 (1991).
22. S. D. Fellicelli, J. C. Heinrich and D. R. Poirier, Simulation of freckles during vertical solidification of binary alloys, *Met. Trans B* **22B,** 847–859 (1991).
23. D. G. Neilson and F. P. Incropera, Unidirectional solidification of a binary alloy and the effects of induced fluid motion, *Int. J. Heat Mass Transfer* **34,** 1717–1732 (1991).
24. R. W. Fox and A. T. McDonald, *Introduction to Fluid Mechanics* (3rd Edn), pp. 210–211. Wiley, New York (1985).
25. A. Hellawell, J. R. Sarazin and R. S. Steube, Channel convection in partly solidified systems, *Phil. Trans. R. Soc. Lond. A* **345,** 507–544 (1993).
26. R. Mehrabian, M. A. Keane and M. C. Flemings, Experiments on macrosegregation and freckle formation, *Met. Trans.* **1,** 3238–3241 (1970).